JAK-STAT pathway activation compromises nephrocyte function in a *Drosophila* high-fat diet model of chronic kidney disease

Yunpo Zhao[1,2], Jianli Duan[1,2], Hannah Seah[1,2], Joyce van de Leemput[1,2], and Zhe Han[1,2,*]

1. Center for Precision Disease Modeling, Department of Medicine, University of Maryland School of Medicine, Baltimore, MD 21201, USA
2. Division of Endocrinology, Diabetes and Nutrition, Department of Medicine, University of Maryland School of Medicine, Baltimore, MD 21201, USA

* Corresponding author: Dr. Zhe Han, Center for Precision Disease Modeling, Department of Medicine, University of Maryland School of Medicine, 670 West Baltimore Street, Baltimore, MD 21201, USA; email: zhan@som.umaryland.edu

Running title: JAK-STAT in high-fat diet dysfunctional nephrocytes

HIGHLIGHTS

- High-fat diet (HFD) disrupt nephrocyte slit diaphragm structure and filtration
- HFD releases fat body adipokine, Upd2, which activates JAK-STAT in nephrocytes
- Genetic/pharmacological inhibition of JAK-STAT reverses HFD nephrocyte dysfunction
- JAK-STAT signaling mediates adipose-nephrocyte axis in HFD-associated nephropathy

IMPACT STATEMENT

Using a *Drosophila* model for chronic kidney disease, Zhao et al. show that a high-fat diet induces excretion of a leptin-like JAK-STAT ligand from the fat body. Thus, driving the adipose-nephrocyte (podocyte equivalent) axis through activated JAK-STAT signaling. These findings link obesity to kidney disease, implicating new avenues for therapeutics.

ABSTRACT

Chronic kidney disease is a major healthy issue and is gaining prevalence. Using a *Drosophila* model for chronic kidney disease we show that a high-fat diet (HFD) disrupts the slit diaphragm filtration structure in nephrocytes, the fly functional equivalent of mammalian podocytes. The structural disruption resulted in reduced filtration function in the affected nephrocytes. We demonstrate that a HFD activates the JAK-STAT pathway in nephrocytes, which has previously been linked to diabetic kidney disease. JAK-STAT activation was initiated by increased expression and release of the adipokine, Upd2, from the fat body. This leptin-like hormone is a known ligand of JAK-STAT. Both genetic and pharmacological inhibition of JAK-STAT restored nephrocyte HFD-associated dysfunction. Altogether, our study reveals the importance of the JAK-STAT signaling pathway in the adipose tissue−nephrocyte axis and its contribution to HFD-associated nephropathy. These findings open new avenues for intervention in treating diabetic nephropathy and chronic kidney disease.

INTRODUCTION

Chronic kidney disease is a prevalent health issue, with an estimated ~12% of people affected worldwide, many of whom are unaware of their condition (Coresh, 2017; US Department of Health and Human Services, Centers for Disease Control and Prevention (Atlanta, GA), 2023). The gradual loss of kidney function results in excess fluid and buildup of metabolic waste compounds. Clinical symptoms include atherosclerosis, chronic inflammation, malnutrition, and insulin resistance among other metabolic imbalances (Serrano et al., 2023). Altogether these lead to increased morbidity and mortality associated with chronic kidney failure (GBD Chronic Kidney Disease Collaboration, 2020). Diabetes, high blood pressure, ageing, obesity, and increased BMI are major risk factors for glomerulopathy and chronic kidney disease (Alizadeh et al., 2019; Berthoux et al., 2013; Bonnet et al., 2001; Coresh, 2017; Hsu et al., 2006; Moorhead et al., 1982; Tsuboi et al., 2013). Notably, patients with primary kidney disease that are also obese have worsened outcomes (Berthoux et al., 2013) and following kidney transplantation patients with increased BMI are at greater risk of adverse outcomes (Curran et al., 2014). with increasing risk as BMI increases (Hsu et al., 2006). The link between dietary fat intake and kidney disease has raised interest into the adipose-renal axis; that is how do bodily fat deposits affect kidney function?

Podocytes from patients with chronic kidney disease contain lipid droplets that store excess fat (Herman-Edelstein et al., 2014; Kimmelstiel and Wilson, 1936), these cause lipotoxicity by disrupting the mitochondria, as well as endocytosis (Lubojemska et al., 2021), a process crucial to the kidney filtration structure (Wang et al., 2021). Studies in rats and mice on a HFD have repeatedly shown that the animals suffer from obesity, diabetes (altered insulin homeostasis), and kidney injury marked by functional (albuminuria; blood accumulation of BUN and creatinine; increased urinary biomarkers of kidney damage) and structural (glomerulopathy with glomerular hypertrophy and focal segmental glomerulosclerosis; fibrosis) deficiencies (Altunkaynak et al., 2008; Ha et al., 2022; Jiang et al., 2005; Kuwahara et al., 2016; Lu et al., 2003; Rangel Silvares et al., 2019; Ruggiero et al., 2011; Sánchez-Navarro et al., 2021; Sun et al., 2020; Szeto et al., 2016; van der Heijden et al., 2015). Like in patients with chronic kidney disease, lipid droplets have been observed in the kidneys of HFD rats and mice (Deji et al., 2009; Jiang et al., 2005; Sun et al., 2020; van der Heijden et al., 2015) and have been associated with dysfunctional cellular systems including oxidative stress, renal inflammation, ER-stress, disruption of mitochondrial dynamics, and impaired autophagy-lysosomal pathway in the cells of the kidneys (Cai et al., 2024; Ha et al., 2022;

Kuwahara et al., 2016; C. Li et al., 2016; Lu et al., 2003; Rangel Silvares et al., 2019; Ruggiero et al., 2011; Sánchez-Navarro et al., 2021; Sun et al., 2020; Szeto et al., 2016; van der Heijden et al., 2015). Altogether, these indicate the involvement of both local and systemic changes (Deji et al., 2009). However, our understanding of the pathways that govern the pathogenic effect of superfluous fat intake on kidney function, as well as how to leverage this knowledge to develop effective therapeutics, remains incomplete.

Recently, an HFD model in *Drosophila* showed lipotoxicity, i.e. lipid droplet accumulation, in the fly nephrocytes (Lubojemska et al., 2021). Nephrocytes share many characteristics with human podocytes, including genetics, molecular pathways, and function (Weavers et al., 2009; Zhang et al., 2013b, 2013a). Both cell types contain highly specialized filtration structures know as slit diaphragms that act in concert with the basement membrane; the fly lacuna channel is similar to the urinary space in the mammalian Bowman's capsule; and, many key proteins for podocyte function are likewise essential for nephrocyte function (van de Leemput et al., 2022; Wang et al., 2021; Weavers et al., 2009; Zhuang et al., 2009). Indeed, fly in vivo nephrocyte models have been successfully used to study a variety of human kidney diseases, including forms of monogenic nephrotic syndrome and steroid-resistant nephrotic syndrome (SRNS) (Ashraf et al., 2013; Bierzynska et al., 2022; Fu et al., 2017; Gee et al., 2015, 2013; Gonçalves et al., 2018; Hermle et al., 2018, 2017; Milosavljevic et al., 2022; Odenthal et al., 2023; Paul et al., 2023; Zhao et al., 2019; Zhu et al., 2017). The recent study using the HFD Drosophila model recapitulated the ectopic lipid droplets and cellular dysfunction observed in chronic kidney disease and found that the adipose-derived triglyceride lipase protects nephrocyte endocytosis under HFD conditions (Lubojemska et al., 2021). Here, we used an HFD *Drosophila melanogaster* model of chronic kidney disease to investigate the role and factors of the adipose-renal axis in chronic kidney disease and identified Upd-activated JAK-STAT signaling as a key component.

RESULTS

High-fat diet (HFD) compromises nephrocyte function

To investigate the effect of superfluous fat consumption on nephrocyte function, newly eclosed flies were fed a normal fat diet (NFD) or a high-fat diet (HFD) for seven days. Then, the flies were subjected to fluorescent dye uptake assays (Weavers et al., 2009; Zhao et al., 2024) to determine pericardial nephrocyte function. HFD leads to enlarged crop (Liao et al., 2020; Zhao et al., 2023a), which was used as an indication of food consistency. Compared to the NFD fed flies, the HFD fed flies showed reduced FITC conjugated albumin (FITC-

albumin, 66 kD) fluorescence (Figure 1A and B). Likewise, HFD feeding significantly reduced 10 kD dextran uptake by the nephrocytes (Figure 1C and D). In line with HFD caused lipid droplet accumulation in the larval nephrocytes (Lubojemska et al., 2021), we observed increased nephrocyte lipid droplets in the adults fed with HFD (Figure 1 – figure supplement 1). Thus, confirming the HFD model in *Drosophila* for studying kidney disease (Lubojemska et al., 2021) and demonstrating that in our hands the consumption of superfluous fat caused nephrocyte uptake dysfunction.

HFD alters nephrocyte morphology

The slit diaphragm (SD) is the fundamental filtration structure of nephrocytes. Thus, given the HFD-induced dysfunctional uptake, we next tested whether the SD is affected by HFD. Therefore we looked at the distribution of polychaetoid (Pyd), the fly homolog of human tight junction protein 1 (TJP1, alias ZO-1) and a key component of the SD filtration unit (van de Leemput et al., 2022). Immunostaining with anti-Pyd antibody showed predominant membrane localization of Pyd in nephrocytes from NFD fed flies. At the cortical surface of NFD nephrocytes, Pyd showed the fingerprint-like pattern characteristic of the SD (Figure 2A). However, in the HFD fed flies, the SD fingerprint-like pattern appeared irregular and Pyd showed an uneven distribution with spots of increased signal intensity (Figure 2A). These might correlate to the trails of Pyd seemingly hanging from the cortical surface inside the HFD nephrocytes, along with cytosolic accumulation of Pyd protein (Figure 2A and B). Next, we used Sns-mRuby3, in which mRuby3 was tagged at the C-terminal of endogenous Sns (Delaney et al., 2024; Zhao et al., 2024), to verify the HFD effect on SD structure. We observed cytoplasm retention of Sns-mRuby3 in the nephrocytes of HFD fed flies (Figure 2 – figure supplement 1). These findings show that a HFD leads to structural disruption of the SD filtration unit in nephrocytes, that likely accounts for the nephrocyte functional deficit observed earlier.

To study the nephrocyte SD and cytoplasmic regions in more detail, we performed transmission electron microscopy (TEM). The nephrocytes of NFD fed flies showed regularly arranged lacuna channels along the cortical surface (Figure 2C). The distance between the lacuna channels was significantly increased in nephrocytes from HFD fed flies (Figure 2C and D). Nephrocytes from both NFD and HFD fed flies showed big subcellular vacuoles (Figure 2E). However, the vacuoles in NFD nephrocytes frequently contained electron dense structures, whereas most vacuoles in HFD nephrocytes were clear (Figure 2E and F). Altogether, these findings demonstrate that a HFD causes significant changes to the nephrocyte and its SD, both at the cortical and subcortical levels.

HFD potentiates the JAK-STAT pathway in nephrocytes

Activity of the Janus kinase/signal transducer and activator of transcription (JAK-STAT) pathway has been linked to diabetic kidney disease (Berthier et al., 2009), likewise it is activated systemically in *Drosophila* in response to a chronic lipid-rich diet (Woodcock et al., 2015). Key components of the JAK-STAT pathway are conserved in fly, including *Signal-transducer and activator of transcription protein at 92E* (*Stat92E*), *hopscotch* (*hop*), *domeless* (*dome*), and *Suppressor of cytokine signaling at 36E* (*Socs36E*) (Figure 3A and B). Therefore, we tested whether the JAK-STAT pathway was activated in the nephrocytes of HFD-fed flies. We used a fluorescent reporter *10xStat92E*-GFP of JAK-STAT pathway activity (Ekas et al., 2006). Low levels of *Stat92E*-GFP fluorescence were detected in the nephrocytes of flies on a regular diet (NFD). However, in nephrocytes from HFD-fed flies, the fluorescence was significantly increased (Figure 3C and D). These findings indicate that the consumption of superfluous fat indeed activates the JAK-STAT pathway in nephrocytes.

Activation of the Janus kinase, Hop, reduces nephrocyte function

Since JAK-STAT signaling has been shown to play an important role during development (Brown et al., 2001; Liu et al., 2009), we wanted to isolate its requirement for mature nephrocyte filtration function. To do this we used a dominant gain-of-function allele of *hop* (*Tumorous-lethal*, *hop.Tum*); a single amino acid change (Gly341Glu) whose expression leads to JAK-STAT pathway activation (Harrison et al., 1995). We expressed *UAS-hop.Tum* specifically in mature nephrocytes using a temperature sensitive *Dot*-Gal4 driver (*Dot*-Gal4*; tub*-Gal80ts, referred to as *Dot*-Gal4ts), known as the TARGET system (McGuire et al., 2004), to turn on expression in adult flies specifically as they are switched to a different environmental temperature (Figure 4A). Overexpression of *hop.Tum* significantly reduced nephrocyte absorption ability in the adults, as shown with reduced FITC-albumin and 10 kD dextran in *Dot*-Gal4ts>UAS-*hop.Tum* nephrocytes compared with control nephrocytes (Figure 4B-E).

To validate these results and remove between-fly variability, both biological and technical, we also tested the effect of JAK-STAT pathway activation in tissue mosaic clones using Flp-out (Delaney et al., 2024; Duan et al., 2020) (Figure 4F). For this technique first instar larvae are exposed to heat shock to activate the Hsp70P transcription factor, which induces *Flippase* (*Flp*). Flp activity in turn, removes the stop-cassette thereby driving Gal4 expression. Gal4 drives the expression of UAS-GFP and UAS-*hop.tum* within the same cell. Thus, *hop.Tum* is only expressed in GFP-labelled nephrocyte clones; whereas, GFP-negative nephrocytes are indicative of no Gal4 being expressed and serve as internal control cells (Figure 4F). In line with the TARGET assays, UAS-*hop.Tum* overexpression

significantly reduced nephrocyte absorption ability in adult flies (Figure 4G and H). These data support a role for JAK-STAT pathway in nephrocyte function.

Depletion of Socs36E, a negative regulator of JAK-STAT, or increased adipokine Upd2, a JAK-STAT ligand, result in decreased nephrocyte function

Next, we looked at additional JAK-STAT pathway components in the context of nephrocyte function. Suppressor of cytokine signaling at 36E (Socs36E) is transcriptionally regulated by Signal-transducer and activator of transcription 92E (Stat92E) and functions as a negative regulator of JAK-STAT signaling (Callus and Mathey-Prevot, 2002; Karsten et al., 2002) (Figure 3B) and it is expressed in the nephrocytes (Figure 3A). Silencing *Socs36E* specifically in nephrocytes (*Dot*-Gal4>*Socs36E*-RNAi) significantly reduced nephrocyte uptake function as evident in significantly decreased FITC-albumin (Figure 5A and B) and 10 kD dextran (Figure 5C and D) fluorescence compared to the control nephrocytes.

In *Drosophila*, the JAK-STAT pathway ligand unpaired (Upd) family is encoded by *upd1*, *upd2*, and *upd3*. These ligands bind to Domeless (Dome), a single-transmembrane receptor, to activate JAK-STAT signaling (Figure 3B). Of these, Upd2 is functionally equivalent to human Leptin and is highly expressed in the fat body, the fly's functional equivalent of vertebrate adipose tissue (Hombria et al., 2005; Rajan et al., 2017; Rajan and Perrimon, 2012). In *Drosophila*, HFD has been shown to upregulate Upd2 expression and secretion (Rajan et al., 2017; Rajan and Perrimon, 2012). In our model, over-expression of Upd2, specifically in the fat body (*ppl*-Gal4 driver; *ppl*-Gal4>*upd2*-GFP), significantly reduced 10 kD dextran uptake in the nephrocytes compared to the control (*ppl*-Gal4/+) (Figure 5E and F), indicating reduced nephrocyte function. Since our *upd2* over-expression line contains *upd2*-GFP, we could not use the FITC-albumin uptake assay, as both signals occupy the same imaging channel. Upd2-GFP signal was found in the nephrocytes in *ppl*-Gal4>*upd2*-GFP flies (Figure 5 - figure supplement 1A), indicating an inter-tissue communication of Upd2-GFP. Notably, Upd2-GFP overexpression in the fat body caused cytoplasm retention of Sns-mRuby3 (Figure 5G and H) and compromised the cortical fingerprint pattern (Figure 5 - figure supplement 1B).

Like the Janus kinase Hop, the negative regulator Socs36E and the ligand adipokine Upd2 are additional JAK-STAT pathway components that are required for nephrocyte function.

HFD-induced nephrocyte functional defects are mitigated by Stat92E-mediated inhibition of JAK-STAT

To determine that JAK-STAT forms a direct link between HFD and nephrocyte dysfunction, we knocked down *Stat92E* (*Stat92E*-IR (Recasens-Alvarez et al., 2017)) in the nephrocytes to disrupt the JAK-STAT signaling pathway (Figure 3B). Deficiency for Stat92E did not affect the uptake function (FITC-albumin or 10 kD dextran) of adult nephrocytes in flies fed a NFD (Figure 6A-D). However, under HFD conditions, in which nephrocytes from control flies showed significantly reduced uptake, *Stat92E* deficient nephrocytes showed FITC-albumin and 10 kD dextran fluorescence restored to NFD levels (Figure 6A-D). We used an independent *Stat92E-RNAi* line in the functional assays and obtained similar results, showing that dextran fluorescence was restored to NFD levels in *Stat92E*-deficient nephrocytes under HFD conditions (Figure 6 - figure supplement 1). Interestingly, under HFD conditions, the cytoplasm retention of Sns-mRuby3 was restored to NFD levels in *Stat92E*-deficient nephrocytes (Figure 6 - figure supplement 2). These findings demonstrate that Stat92E, and by extension the JAK-STAT pathway, is required for the nephrocyte dysfunction induced by HFD.

HFD-induced nephrocyte functional defects can be attenuated by methotrexate treatment

Methotrexate suppresses STAT activation; it inhibits the phosphorylation of JAK which is necessary for JAK-STAT pathway activation, and was shown to do so without affecting other phosphorylation-dependent pathways (Thomas et al., 2015). In our model system, methotrexate treatment (10 µM; 60 min) reduced levels of Stat92E (10xStat92E-GFP) in the nephrocytes (Figure 7 - figure supplement 1). Stat92E is a key component of the pathway, its reduction is indicative of decreased JAK-STAT signaling. Next, we treated flies on NFD or HFD with 10 µM methotrexate (60 min incubation; ex vivo) to study the effect of pharmacological JAK-STAT inhibition on nephrocyte function. In nephrocytes from control flies on a regular diet (NFD), the methotrexate treatment had no effect on uptake of FITC-albumin or 10 kD dextran (Figure 7A-D). However, in flies on a HFD, treatment with methotrexate led to significantly increased nephrocyte FITC-albumin and 10 kD dextran uptake, restoring levels to those observed in control fly NFD nephrocytes (Figure 7A-D). We asked whether methotrexate treatment has an effect on Sns-mRuby3 subcellular distribution. In line with our prediction, under HFD conditions, pharmacological JAK-STAT inhibition restored Sns-mRuby3 distribution to NFD levels (Figure 7 - figure supplement 2). Thus, like the genetic intervention (*Stat92E* inhibition; Figure 6), pharmacological intervention with the JAK-STAT inhibitor methotrexate restored nephrocyte function caused by HFD. These findings support the notion that HFD-induced nephrocyte dysfunction is mediated by the JAK-STAT signaling pathway.

Keywords
JAK-STAT; Upd2; Leptin; high-fat diet; nephropathy; chronic kidney disease; *Drosophila*

DISCUSSION

A recent publication showed that flies fed a HFD can recapitulate key features of chronic kidney disease, including lipid droplet formation, altered mitochondria dynamics, and endocytosis defects observed as reduced uptake of dextran and albumin (Lubojemska et al., 2021). This previous study found that excess fatty acids, a sign of lipotoxicity, due to a HFD are released from adipose tissue into circulation, then filtered out by the nephrocytes by receptor-mediated endocytosis, at which point the fatty acids accumulate in the lipid droplets (Lubojemska et al., 2021); like those observed in the podocytes of patients with chronic kidney disease (Herman-Edelstein et al., 2014; Kimmelstiel and Wilson, 1936). Notably, lipid droplet lipolysis and PGC1α could counteract the HFD-induced disrupted endocytosis in the nephrocytes via the mitochondria (Lubojemska et al., 2021). This demonstrated one mechanism by which excess lipid droplets, due to HFD, can disrupt nephrocyte kidney function. Here, we likewise used a HFD *Drosophila* model to study chronic kidney disease and revealed another mechanism by which HFD affects both nephrocyte uptake function and morphology of its filtration structure, the slit diaphragm. HFD upregulates the expression of the adipokine Upd2, the functional homolog to human Leptin, which activates the JAK-STAT pathway (Rajan and Perrimon, 2012; Zhao et al., 2023b). Of note, a previous study has shown that Stat1 exerts a repressive effect on PGC1α transcription (Sisler et al., 2015). These observations suggest a potential mechanistic interaction between Jak/Stat signaling and PGC1α regulation. Our data show this also holds true in the nephrocytes, and as such compromises nephrocyte function (Figure 7E). These findings support obesity as a causal factor in chronic kidney disease.

Of note, in early stage diabetic kidney disease, JAK-STAT pathway genes are upregulated in patient podocytes (Berthier et al., 2009). In a rat diabetic model, treatment with a JAK-STAT inhibitor (AG-490) reduced proteinuria (Banes et al., 2004); and, overexpression of JAK2 in diabetic mouse podocytes elevated JAK-STAT pathway activity and exacerbated diabetic kidney disease (Zhang et al., 2017). These findings, like ours that showed effective treatment of HFD nephropathy using the JAK-STAT inhibitor (methotrexate), support the involvement of the JAK-STAT pathway in HFD-related chronic kidney disease. They also demonstrate that this pathological effect is conserved from flies to mammals. In fact, a phase 2 clinical trial demonstrated that the small molecule baricitinib, a selective JAK1 and JAK2

inhibitor, effectively lowered albuminuria in patients with type 2 diabetes and diabetic kidney disease (Tuttle et al., 2018). Altogether these studies support JAK-STAT inhibition as a therapeutic intervention for nephropathy associated with superfluous fat intake (Brosius et al., 2016). The conserved disease mechanism makes the HFD fly model a valuable platform to screen JAK-STAT inhibitors for their efficacy to treat chronic kidney disease. The fly findings showed a direct JAK-STAT link at the adipose tissue−nephrocyte axis leads to nephrocyte dysfunction; via HFD upregulated expression of the adipokine Upd2, which activates the JAK-STAT pathway (Rajan and Perrimon, 2012) (Figure 7E). In support, like in our fly model, increased leptin has been observed in obese patients (Considine et al., 1996) and in patients with chronic renal failure (Heimbürger et al., 1997).

Finally, while growing evidence demonstrates that a pharmacological block of the JAK-STAT pathway could effectively treat nephropathy, for decades, the first-line treatment for obesity-related glomerulopathy has been RAS inhibitors (Jiang et al., 2023). Their beneficial effects stemming from lowering blood pressure and by lowering the estimated glomerular filtration rate (eGFR) (Banerjee et al., 2022; Yamout et al., 2014). One such inhibitor, telmisartan, targets RAS by blocking the angiotensin (Ang) II receptor and was shown effective in treating nephropathy in a rat model of metabolic syndrome (HFD-fed rats) (H. Li et al., 2016). Notably, telmisartan treatment decreased leptin release from adipose tissue, thereby supporting our model and implicating a hitherto unknown mechanism contributes to leptin-associated nephropathy in metabolic syndrome. In addition, our findings could have implications for lupus nephritis, an inflammatory kidney disease associated with the autoimmune disease systemic lupus erythematosus. Patients with this complication show activated JAK-STAT and elevated leptin, regulated by Sterol regulatory element bending transcription factor 1 (SREBF1) which is involved in lipogenesis (Hao et al., 2013). Already, phase 2/3 clinical trials are underway to study the efficacy of JAK inhibitors in treating lupus nephritis (Huo et al., 2023). Our data indicate a possible second pathway could contribute, by direct leptin stimulation of JAK-STAT caused by the dysregulated fat body, warranting further investigation.

Altogether, our study expands our understanding of chronic kidney disease associated with superfluous fat intake and provides new avenues for therapeutic strategies.

MATERIALS AND METHODS

Key resources table

REAGENT or RESOURCE	SOURCE	IDENTIFIER
Antibodies		
Chicken anti-GFP	Abcam	Cat. ab13970; RRID:AB_300798
Mouse monoclonal anti-Pyd	Developmental Studies Hybridoma Bank (DSHB)	RRID:AB_2618043
Goat anti-mouse Alexa fluor 488	Invitrogen	Cat. A11029; RRID:AB_2534088
Goat anti-chicken Alexa fluor 488	Invitrogen	Cat. A11039; AB_2534096
Chemicals, Peptides, and Recombinant Proteins		
DAPI	Thermo Fisher Scientific	Cat. D1306
Methotrexate	Sigma-Aldrich	Cas. 06563
10 kD Texas Red-dextran	Thermo Fisher Scientific	Cas. D1828
FITC-albumin solution	Sigma	Cas. A9771
Experimental Models: Organisms/Strains		
Drosophila melanogaster: w^{1118}	Bloomington Drosophila Stock Center (BDSC)	RRID: BDSC_3605
Drosophila melanogaster: *Dot*-Gal4	BDSC	RRID: BDSC_67608
Drosophila melanogaster: *ppl*-Gal4	BDSC	RRID: BDSC_58768
Drosophila melanogaster: *tub*-Gal80ts	BDSC	RRID: BDSC_7017
Drosophila melanogaster: *10XStat92E*-GFP	BDSC	RRID: BDSC_26198
Drosophila melanogaster: *Stat92E-IR_#2*	BDSC	RRID: BDSC_33637
Drosophila melanogaster: *Socs36E*-IR	BDSC	RRID: BDSC_35036
Drosophila melanogaster: *Stat92E-IR*	Vienna *Drosophila* Resource Center (VDRC)	VDRC_106980
Drosophila melanogaster: UAS-*hop.Tum*	Harrison, et.al., 1955	N/A
Drosophila melanogaster: *sns-mRuby3*	Delaney, et. al., 2024	N/A
Drosophila melanogaster: UAS-*upd2:GFP*	Hombria, et.al., 2005	N/A
Drosophila melanogaster: *hs-Flp*^{122}; UAS-*Flp*^{JD1}/CyO, *Act-GFP*^{JMR1}; *Act5C>CD2>Gal4*^{S}, UAS-*mCD8-GFP*^{LL6}/TM6b	Zhao, et.al., 2005	N/A
Software and Algorithms		
FIJI (ImageJ)	Schneider et al., 2012; https://imagej.net/Fiji/Downloads	Fiji-macOS
Adobe Illustrator	https://www.adobe.com/	Adobe Illustrator 2022
GraphPad Prism	https://www.graphpad.com/scientific-software/prism/	GraphPad Prism 9

Drosophila **husbandry**

Fly lines were reared on a normal fat diet (NFD; Nutri-Fly German formula; Genesee Scientific, San Diego, CA) or a high-fat diet (HFD; NFD supplemented with 14% coconut oil),

under standard conditions (25°C, 60% humidity, 12h:12h dark:light cycle), unless otherwise stated.

Drosophila stocks *w*^{1118} (BDSC_3605), *Dot*-Gal4 (BDSC_67608), *ppl*-Gal4 (BDSC_58768), *tub*-Gal80ts (BDSC_7017), *10XStat92E*-GFP (BDSC_26198), UAS-*Stat92E*-RNAi_#2 (BDSC_33637), and UAS-*Socs36E*-RNAi (BDSC_35036) were obtained from the Bloomington Drosophila Stock Center (BDSC). UAS-*Stat92E*-RNAi (VDRC_106980) was obtained from the Vienna Drosophila Resource Center (VDRC). UAS-*hop.Tum* was kindly provided by Prof. Norbert Perrimon (Harvard Medical School, Boston, MA; Howard Hughes Medical Institute, Boston, MA). UAS-*upd2:GFP* has been previously described (Hombria et al., 2005) and was kindly provided by Prof. Ylva Engström (Stockholm University, Stockholm, Sweden). The Flp-out line *hs-Flp*^{122}; UAS-*Flp*^{JD1}/CyO, *Act-GFP*^{JMR1}; *Act5C>CD2>Gal4*^{S}, UAS-*mCD8-GFP*^{LL6}/TM6b was generated previously (Zhao et al., 2015).

FITC-albumin and 10 kD dextran uptake assays

Nephrocyte functional assays were performed ex vivo at room temperature, following a previously described method (Wen et al., 2020) with minor changes. *Drosophila* females were dissected in Schneider's Drosophila Medium (Thermo Fisher Scientific, MA), then incubated in a 10 kD Texas Red-dextran solution (0.05 mg/mL; D1828, Thermo Fisher Scientific, MA) in Schneider's Drosophila Medium (Thermo Fisher Scientific, MA) for 20 min, or a FITC-albumin solution (10 mM; Sigma, A9771) in Schneider's Drosophila Medium (Thermo Fisher Scientific, MA) for 5 min. The specimens were washed in artificial hemolymph twice, followed by fixation in 4% paraformaldehyde (PFA) for 60 min. Then the fixed specimens were washed thrice for 5 min in 1x phosphate buffered saline (1xPBS; pH 7.4) and mounted using Vectashield mounting medium (H-1000, Vector Laboratories, CA). FITC-albumin and 10 kD dextran specimens were imaged using a ZEISS LSM900 confocal microscope with ZEISS Zen acquisition software (blue edition; version 3.0) using a 20× Plan-Apochromat 0.8 N.A. air objective (ZEISS, Oberkochen, Germany). For quantitative comparison of fluorescence intensities, setting for the control condition were chosen to avoid oversaturation (using Range Indicator in ZEN blue; limiting the observed red dots to avoid oversaturation), then applied across the images for all samples/conditions within the assay. The fluorescence intensity of FITC-albumin and 10 kD dextran nephrocytes was determined using Fiji software (Image J (Schneider et al., 2012) , version 2.9.0/1.53t; National Institutes of Health, Bethesda, MD). For quantitation, for each genotype, the relative fluorescence intensity of 30 nephrocytes from 6 female flies (5 nephrocytes/fly) was analyzed.

Immunochemistry

Immunostaining was performed as previously reported (Zhao et al., 2022) with minor changes. Flies were briefly rinsed in 95% ethanol and dissected in 1xPBS at room temperature. Specimens were incubated in primary antibodies overnight at 4 °C. The incubations in secondary antibodies were performed either overnight at 4 °C or for 2 hours at room temperature. The following antibodies were used: chicken anti-GFP (1:1,000; ab13970, RRID:AB_300798, Abcam, Cambridge, UK), mouse monoclonal anti-Pyd (1:100; RRID:AB_2618043, Developmental Studies Hybridoma Bank, IA), goat anti-mouse Alexa fluor 488 (1:500; A11029, RRID:AB_2534088, Invitrogen, Eugene, OR), and goat anti-chicken Alexa fluor 488 (1:500; A11039, AB_2534096, Invitrogen, Eugene, OR). DAPI (0.5 mg/ml in PBST (0.2% Triton-x 100 in 1xPBS); D1306, Thermo Fisher Scientific, MA) was used to visualize the nuclei. The nephrocytes were imaged using a ZEISS LSM900 confocal microscope (under airyscan mode for Pyd images) with ZEISS ZEN acquisition software (blue edition; version 3.0) and a 63× Plan-Apochromat 1.4 N.A. oil objective (ZEISS, Oberkochen, Germany). For quantitative comparison of fluorescence intensities, setting for the control condition were chosen to avoid oversaturation (using Range Indicator in ZEN blue; limiting the observed red dots to avoid oversaturation), then applied across the images for all samples/conditions within the assay. Image J (Schneider et al., 2012) was used for image processing (version 2.9.0/1.53t; National Institutes of Health, Bethesda, MD). Typically, six flies were imaged per condition, representative images for each are displayed in the figures.

Transmission electron microscopy (TEM)

TEM was performed using standardized procedures. In brief, female adults (7-days-old) were dissected in Schneider's Drosophila Medium (Thermo Fisher Scientific, MA). The heart tube and the attached nephrocytes were dissected, removed, and fixed using Sorensen phosphate buffer (2% PFA, 2.5% EM grade glutaraldehyde, 2mM $CaCl_2$, 0.1 M NaOH; provided by the Electron Microscopy Core Imaging Facility at the Center for Innovative Biomedical Resources (CIBR), University of Maryland School of Medicine, MD). The processed specimens were imaged using a Philips CM100 TEM, carried out at the Electron Microscopy Core Imaging Facility at the Center for Innovative Biomedical Resources (CIBR) (University of Maryland School of Medicine, MD). The LC-LC distances were measured using the Straight Line tool in Fiji (Image J (Schneider et al., 2012) , version 2.9.0/1.53t; National Institutes of Health, Bethesda, MD) to connect two adjacent lacuna channels (LCs); a straight line was drawn from the middle of the first LC to the middle of the sixth LC, covering five LC-LC intervals on a TEM image, then the measure function was used to obtain the distance value. In total 60 LC-LC distances were measure per condition in 10 nephrocytes from six 7-day-old female flies. The presence of a dark electron dense structure

in the vacuoles was manually determined and counted in images obtained from 12 nephrocytes for NFD and 29 nephrocytes from HFD from six 7-day-old female flies.

Tissue mosaic analysis

Flp-out clone (Struhl and Basler, 1993) induction was performed as previously described (Duan et al., 2020). In brief, female virgins of *hs-Flp*^{122}; UAS-*Flp*^{JD1}/CyO, *Act-GFP*^{JMR1}; *Act5C>CD2>Gal4*^{S}, UAS-*mCD8-GFP*^{LL6}/TM6b (Zhao et al., 2015) were crossed with UAS-*hop.Tum* males. The embryos were collected for 24 hours. First instar larvae (24 hrs after embryo collection) received a 10 min heat shock in a 37°C water bath to induce the mosaic clones. After the heat shock, the larvae were maintained at 25°C. One-day-old female adults were subjected to the 10 kD dextran functional assay (described above). The GFP-positive nephrocyte clones and their neighboring nephrocytes were analyzed.

Methotrexate treatment

Methotrexate (06563, Sigma-Aldrich, MO) was dissolved in DMSO to make a 10mM stock solution. Flies were dissected as described for the nephrocyte functional assays. The dorsal cuticle (with nephrocytes) was transferred to methotrexate solution (10 μM) in Schneider's Drosophila Medium (Thermo Fisher Scientific, MA) and incubated at room temperature for 60 min. The samples incubated in Schneider's Medium supplemented with DMSO vehicle were used a control. The specimens were rinsed with Schneider's Drosophila Medium (Thermo Fisher Scientific, MA), then subjected to a functional assay or fixed in 4% PFA for immunochemistry.

Nie Red staining

Newly eclosed *w*^{1118} flies were fed either a high-fat diet (HFD) or a control diet (CD) for 7 days before staining for lipid droplets using Nile Red. For Nile Red staining, nephrocytes were dissected in 1× PBS and fixed in 4% paraformaldehyde for 1 hour at room temperature. The samples were then washed three times with 1× PBS for 5 minutes each, followed by incubation with 0.1 μg/mL Nile Red (HY-D0718, MedChemExpress) for 10 minutes at room temperature. Afterward, the samples were rinsed three more times with 1× PBS for 5 minutes each.

Data analyses and figure preparation

Image J (Schneider et al., 2012) (version 2.9.0/1.53t; National Institutes of Health, Bethesda, MD) was used to process the raw data of confocal images and to measure the relative fluorescence intensity. The data sets were tested for normality using the Shapiro-Wilk test and plotted using GraphPad Prism9 software (version 9.5.1). Normally distributed data were

analyzed by the two-tailed Student's t-test, or by two-way ANOVA with Sidak correction. $P < 0.05$ was considered significant. The figures were arranged using Adobe Illustrator software (version 2022 26.2.1).

ACKNOWLEDGMENTS

We thank the Bloomington Drosophila Stock Center (BDSC) based at Indiana University (Bloomington, IN), the Vienna Drosophila Resource Center (VDRC) based at Vienna BioCenter (Vienna, Austria), Prof. Norbert Perrimon (Harvard Medical School, Boston, MA; Howard Hughes Medical Institute, Boston, MA), and Prof. Ylva Engström (Stockholm University, Stockholm, Sweden) for sharing *Drosophila* stocks; and the Developmental Studies Hybridoma Bank (DSHB) based at the University of Iowa (Iowa City, IA) for the providing the antibodies. Finally, we thank the Electron Microscopy Core Imaging Facility at the Center for Innovative Biomedical Resources (CIBR) (University of Maryland School of Medicine, MD, USA) for their support in TEM image acquisition.

FUNDING

This work was support by National Institutes of Health grants R01-DK098410 (Z.H.).

DATA AVAILABILITY

All relevant data can be found within the article and its supplementary information. Requests for resources and reagents related to this manuscript should be directed to and will be fulfilled by the lead contact, Dr. Zhe Han (zhan@som.umaryland.edu).

AUTHOR CONTRIBUTIONS

Z.H. and Y.Z. designed the study; Y.Z., J.D. and H.S. carried out the experiments; Y.Z., J.D., J.vdL., and Z.H. analyzed and interpreted the data; Y.Z. prepared the figures; Y.Z., J.vdL., and Z.H. drafted and revised the manuscript; the manuscript has been critically reviewed and the final version approved by all authors. **ORCIDs:** Yunpo Zhao (0000-0002-7942-

3406); Jianli Duan (0000-0001-7347-4774); Joyce van de Leemput (0000-0003-1903-7295); Zhe Han (0000-0002-5177-7798)

DISCLOSURES

The authors declare no competing interests.

REFERENCES

Alizadeh S, Esmaeili H, Alizadeh M, Daneshzad E, Sharifi L, Radfar H, Radaei MK. 2019. Metabolic phenotypes of obese, overweight, and normal weight individuals and risk of chronic kidney disease: a systematic review and meta-analysis. *Arch Endocrinol Metab* **63**:427–437.

Altunkaynak ME, Ozbek E, Altunkaynak BZ, Can I, Unal D, Unal B. 2008. The effects of high-fat diet on the renal structure and morphometric parametric of kidneys in rats. *J Anat* **212**:845–852.

Ashraf S, Gee HY, Woerner S, Xie LX, Vega-Warner V, Lovric S, Fang H, Song X, Cattran DC, Avila-Casado C, Paterson AD, Nitschké P, Bole-Feysot C, Cochat P, Esteve-Rudd J, Haberberger B, Allen SJ, Zhou W, Airik R, Otto EA, Barua M, Al-Hamed MH, Kari JA, Evans J, Bierzynska A, Saleem MA, Böckenhauer D, Kleta R, El Desoky S, Hacihamdioglu DO, Gok F, Washburn J, Wiggins RC, Choi M, Lifton RP, Levy S, Han Z, Salviati L, Prokisch H, Williams DS, Pollak M, Clarke CF, Pei Y, Antignac C, Hildebrandt F. 2013. ADCK4 mutations promote steroid-resistant nephrotic syndrome through CoQ10 biosynthesis disruption. *J Clin Invest* **123**:5179–5189.

Banerjee D, Winocour P, Chowdhury TA, De P, Wahba M, Montero R, Fogarty D, Frankel AH, Karalliedde J, Mark PB, Patel DC, Pokrajac A, Sharif A, Zac-Varghese S, Bain S, Dasgupta I, Association of British Clinical Diabetologists and The Renal Association. 2022. Management of hypertension and renin-angiotensin-aldosterone system blockade in adults with diabetic kidney disease: Association of British Clinical Diabetologists and the Renal Association UK guideline update 2021. *BMC Nephrol* **23**:9.

Banes AK, Shaw S, Jenkins J, Redd H, Amiri F, Pollock DM, Marrero MB. 2004. Angiotensin II blockade prevents hyperglycemia-induced activation of JAK and STAT proteins in diabetic rat kidney glomeruli. *Am J Physiol Renal Physiol* **286**:F653-9.

Berthier CC, Zhang H, Schin M, Henger A, Nelson RG, Yee B, Boucherot A, Neusser MA, Cohen CD, Carter-Su C, Argetsinger LS, Rastaldi MP, Brosius FC, Kretzler M. 2009. Enhanced Expression of Janus Kinase–Signal Transducer and Activator of Transcription Pathway Members in Human Diabetic Nephropathy. *Diabetes* **58**:469–477.

Berthoux F, Mariat C, Maillard N. 2013. Overweight/obesity revisited as a predictive risk factor in primary IgA nephropathy. *Nephrol Dial Transplant* **28 Suppl 4**:iv160-6.

Bierzynska A, Bull K, Miellet S, Dean P, Neal C, Colby E, McCarthy HJ, Hegde S, Sinha MD, Bugarin Diz C, Stirrups K, Megy K, Mapeta R, Penkett C, Marsh S, Forrester N, Afzal M, Stark H, BioResource N, Williams M, Welsh GI, Koziell AB, Hartley PS, Saleem MA. 2022. Exploring the relevance of NUP93 variants in steroid-resistant nephrotic syndrome using next generation sequencing and a fly kidney model. *Pediatr Nephrol* **37**:2643–2656.

Bonnet F, Deprele C, Sassolas A, Moulin P, Alamartine E, Berthezène F, Berthoux F. 2001. Excessive body weight as a new independent risk factor for clinical and pathological progression in primary IgA nephritis. *Am J Kidney Dis* **37**:720–727.

Brosius FC, Tuttle KR, Kretzler M. 2016. JAK inhibition in the treatment of diabetic kidney disease. *Diabetologia* **59**:1624–1627.

Brown S, Hu N, Hombría JC. 2001. Identification of the first invertebrate interleukin JAK/STAT receptor, the Drosophila gene domeless. *Curr Biol* **11**:1700–1705.

Cai M-Y, Jiang X-S, Wei Y-X, Wen R-Z, Du X-G. 2024. Role of TFEB-autophagy lysosomal pathway in palmitic acid induced renal tubular epithelial cell injury. *Biochem Biophys Res Commun* **696**:149472.

Callus BA, Mathey-Prevot B. 2002. SOCS36E, a novel Drosophila SOCS protein, suppresses JAK/STAT and EGF-R signalling in the imaginal wing disc. *Oncogene* **21**:4812–4821.

Considine RV, Sinha MK, Heiman ML, Kriauciunas A, Stephens TW, Nyce MR, Ohannesian JP, Marco CC, McKee LJ, Bauer TL. 1996. Serum immunoreactive-leptin concentrations in normal-weight and obese humans. *N Engl J Med* **334**:292–295.

Coresh J. 2017. Update on the Burden of CKD. *J Am Soc Nephrol* **28**:1020–1022.

Curran SP, Famure O, Li Y, Kim SJ. 2014. Increased recipient body mass index is associated with acute rejection and other adverse outcomes after kidney transplantation. *Transplantation* **97**:64–70.

Deji N, Kume S, Araki S-I, Soumura M, Sugimoto T, Isshiki K, Chin-Kanasaki M, Sakaguchi M, Koya D, Haneda M, Kashiwagi A, Uzu T. 2009. Structural and functional changes in the kidneys of high-fat diet-induced obese mice. *American Journal of Physiology-Renal Physiology* **296**:F118–F126.

Delaney M, Zhao Y, van de Leemput J, Lee H, Han Z. 2024. Actin cytoskeleton and integrin components are interdependent for slit diaphragm maintenance in Drosophila nephrocytes. *Cells* **13**:1350.

Duan J, Zhao Y, Li H, Habernig L, Gordon MD, Miao X, Engstrom Y, Buttner S. 2020. Bab2 Functions as an Ecdysone-Responsive Transcriptional Repressor during Drosophila Development. *Cell Rep* **32**:107972.

Ekas LA, Baeg G-H, Flaherty MS, Ayala-Camargo A, Bach EA. 2006. JAK/STAT signaling promotes regional specification by negatively regulating wingless expression in Drosophila. *Development* **133**:4721–4729.

Fu Y, Zhu J-Y, Richman A, Zhao Z, Zhang F, Ray PE, Han Z. 2017. A Drosophila model system to assess the function of human monogenic podocyte mutations that cause nephrotic syndrome. *Hum Mol Genet* **26**:768–780.

GBD Chronic Kidney Disease Collaboration. 2020. Global, regional, and national burden of chronic kidney disease, 1990-2017: a systematic analysis for the Global Burden of Disease Study 2017. *Lancet* **395**:709–733.

Gee HY, Saisawat P, Ashraf S, Hurd TW, Vega-Warner V, Fang H, Beck BB, Gribouval O, Zhou W, Diaz KA, Natarajan S, Wiggins RC, Lovric S, Chernin G, Schoeb DS, Ovunc B, Frishberg Y, Soliman NA, Fathy HM, Goebel H, Hoefele J, Weber LT, Innis JW, Faul C, Han Z, Washburn J, Antignac C, Levy S, Otto EA, Hildebrandt F. 2013. ARHGDIA mutations cause nephrotic syndrome via defective RHO GTPase signaling. *J Clin Invest* **123**:3243–3253.

Gee HY, Zhang F, Ashraf S, Kohl S, Sadowski CE, Vega-Warner V, Zhou W, Lovric S, Fang H, Nettleton M, Zhu J-Y, Hoefele J, Weber LT, Podracka L, Boor A, Fehrenbach H, Innis JW, Washburn J, Levy S, Lifton RP, Otto EA, Han Z, Hildebrandt F. 2015. KANK deficiency leads to podocyte dysfunction and nephrotic syndrome. *J Clin Invest* **125**:2375–2384.

Gonçalves S, Patat J, Guida MC, Lachaussée N, Arrondel C, Helmstädter M, Boyer O, Gribouval O, Gubler M-C, Mollet G, Rio M, Charbit M, Bole-Feysot C, Nitschke P, Huber TB, Wheeler PG, Haynes D, Juusola J, Billette de Villemeur T, Nava C, Afenjar A, Keren B, Bodmer R, Antignac C, Simons M. 2018. A homozygous KAT2B

variant modulates the clinical phenotype of ADD3 deficiency in humans and flies. *PLoS Genet* **14**:e1007386.

Ha S, Yang Y, Kim BM, Kim J, Son M, Kim D, Yu HS, Im D-S, Chung HY, Chung KW. 2022. Activation of PAR2 promotes high-fat diet-induced renal injury by inducing oxidative stress and inflammation. *Biochim Biophys Acta Mol Basis Dis* **1868**:166474.

Hao J, Zhang Y-J, Lv X, Xu N, Liu Q-J, Zhao S, Feng X-J, Xing L-L, Kang P-P, Li G-Y, Liu S-X. 2013. IFN-γ induces lipogenesis in mouse mesangial cells via the JAK2/STAT1 pathway. *Am J Physiol Cell Physiol* **304**:C760-7.

Harrison DA, Binari R, Nahreini TS, Gilman M, Perrimon N. 1995. Activation of a Drosophila Janus kinase (JAK) causes hematopoietic neoplasia and developmental defects. *EMBO J* **14**:2857–2865.

Heimbürger O, Lönnqvist F, Danielsson A, Nordenström J, Stenvinkel P. 1997. Serum immunoreactive leptin concentration and its relation to the body fat content in chronic renal failure. *J Am Soc Nephrol* **8**:1423–1430.

Herman-Edelstein M, Scherzer P, Tobar A, Levi M, Gafter U. 2014. Altered renal lipid metabolism and renal lipid accumulation in human diabetic nephropathy. *J Lipid Res* **55**:561–572.

Hermle T, Braun DA, Helmstädter M, Huber TB, Hildebrandt F. 2017. Modeling Monogenic Human Nephrotic Syndrome in the Drosophila Garland Cell Nephrocyte. *J Am Soc Nephrol* **28**:1521–1533.

Hermle T, Schneider R, Schapiro D, Braun DA, van der Ven AT, Warejko JK, Daga A, Widmeier E, Nakayama M, Jobst-Schwan T, Majmundar AJ, Ashraf S, Rao J, Finn LS, Tasic V, Hernandez JD, Bagga A, Jalalah SM, El Desoky S, Kari JA, Laricchia KM, Lek M, Rehm HL, MacArthur DG, Mane S, Lifton RP, Shril S, Hildebrandt F. 2018. GAPVD1 and ANKFY1 Mutations Implicate RAB5 Regulation in Nephrotic Syndrome. *J Am Soc Nephrol* **29**:2123–2138.

Hombria JC, Brown S, Hader S, Zeidler MP. 2005. Characterisation of Upd2, a Drosophila JAK/STAT pathway ligand. *Dev Biol* **288**:420–433.

Hsu C-Y, McCulloch CE, Iribarren C, Darbinian J, Go AS. 2006. Body mass index and risk for end-stage renal disease. *Ann Intern Med* **144**:21–28.

Huo R, Huang X, Yang Y, Lin J. 2023. Potential Use of Janus Kinase Inhibitors in the Treatment of Systemic Lupus Erythematosus. *J Inflamm Res* **16**:1471–1478.

Jiang T, Wang Z, Proctor G, Moskowitz S, Liebman SE, Rogers T, Lucia MS, Li J, Levi M. 2005. Diet-induced obesity in C57BL/6J mice causes increased renal lipid accumulation and glomerulosclerosis via a sterol regulatory element-binding protein-1c-dependent pathway. *J Biol Chem* **280**:32317–32325.

Jiang Z, Wang Y, Zhao X, Cui H, Han M, Ren X, Gang X, Wang G. 2023. Obesity and chronic kidney disease. *Am J Physiol Endocrinol Metab* **324**:E24–E41.

Karsten P, Häder S, Zeidler MP. 2002. Cloning and expression of Drosophila SOCS36E and its potential regulation by the JAK/STAT pathway. *Mech Dev* **117**:343–346.

Kimmelstiel P, Wilson C. 1936. Intercapillary lesions in the glomeruli of the kidney. *Am J Pathol* **12**:83-98.7.

Kuwahara S, Hosojima M, Kaneko R, Aoki H, Nakano D, Sasagawa T, Kabasawa H, Kaseda R, Yasukawa R, Ishikawa T, Suzuki A, Sato H, Kageyama S, Tanaka T, Kitamura N, Narita I, Komatsu M, Nishiyama A, Saito A. 2016. Megalin-Mediated Tubuloglomerular Alterations in High-Fat Diet-Induced Kidney Disease. *J Am Soc Nephrol* **27**:1996–2008.

Li C, Lin Y, Luo R, Chen S, Wang F, Zheng P, Levi M, Yang T, Wang W. 2016. Intrarenal renin-angiotensin system mediates fatty acid-induced ER stress in the kidney. *Am J Physiol Renal Physiol* **310**:F351-63.

Li H, Li M, Liu P, Wang Y, Zhang H, Li Hongbin, Yang S, Song Y, Yin Y, Gao L, Cheng S, Cai J, Tian G. 2016. Telmisartan Ameliorates Nephropathy in Metabolic Syndrome by Reducing Leptin Release From Perirenal Adipose Tissue. *Hypertension* **68**:478–490.

Liao S, Amcoff M, Nassel DR. 2020. Impact of high-fat diet on lifespan, metabolism, fecundity and behavioral senescence in Drosophila. *Insect Biochem Mol Biol* **2020/11/11**:103495.

Liu Y-H, Jakobsen JS, Valentin G, Amarantos I, Gilmour DT, Furlong EEM. 2009. A systematic analysis of Tinman function reveals Eya and JAK-STAT signaling as essential regulators of muscle development. *Dev Cell* **16**:280–291.

Lu J, Bankovic-Calic N, Ogborn M, Saboorian MH, Aukema HM. 2003. Detrimental Effects of a High Fat Diet in Early Renal Injury Are Ameliorated by Fish Oil in Han:SPRD-cy Rats. *J Nutr* **133**:180–186.

Lubojemska A, Stefana MI, Sorge S, Bailey AP, Lampe L, Yoshimura A, Burrell A, Collinson L, Gould AP. 2021. Adipose triglyceride lipase protects renal cell endocytosis in a Drosophila dietary model of chronic kidney disease. *PLoS Biol* **19**:e3001230.

McGuire SE, Mao Z, Davis RL. 2004. Spatiotemporal gene expression targeting with the TARGET and gene-switch systems in Drosophila. *Sci STKE* **2004**:l6.

Milosavljevic J, Lempicki C, Lang K, Heinkele H, Kampf LL, Leroy C, Chen M, Gerstner L, Spitz D, Wang M, Knob AU, Kayser S, Helmstädter M, Walz G, Pollak MR, Hermle T. 2022. Nephrotic Syndrome Gene TBC1D8B Is Required for Endosomal Maturation and Nephrin Endocytosis in Drosophila. *J Am Soc Nephrol* **33**:2174–2193.

Moorhead JF, Chan MK, El-Nahas M, Varghese Z. 1982. Lipid nephrotoxicity in chronic progressive glomerular and tubulo-interstitial disease. *Lancet* **2**:1309–1311.

Odenthal J, Dittrich S, Ludwig V, Merz T, Reitmeier K, Reusch B, Höhne M, Cosgun ZC, Hohenadel M, Putnik J, Göbel H, Rinschen MM, Altmüller J, Koehler S, Schermer B, Benzing T, Beck BB, Brinkkötter PT, Habbig S, Bartram MP. 2023. Modeling of ACTN4-Based Podocytopathy Using Drosophila Nephrocytes. *Kidney Int Rep* **8**:317–329.

Paul MS, Duncan AR, Genetti CA, Pan H, Jackson A, Grant PE, Shi J, Pinelli M, Brunetti-Pierri N, Garza-Flores A, Shahani D, Saneto RP, Zampino G, Leoni C, Agolini E, Novelli A, Blümlein U, Haack TB, Heinritz W, Matzker E, Alhaddad B, Abou Jamra R, Bartolomaeus T, AlHamdan S, Carapito R, Isidor B, Bahram S, Ritter A, Izumi K, Shakked BP, Barel O, Ben Zeev B, Begtrup A, Carere DA, Mullegama SV, Palculict TB, Calame DG, Schwan K, Aycinena ARP, Traberg R, Genomics England Research Consortium, Douzgou S, Pirt H, Ismayilova N, Banka S, Chao H-T, Agrawal PB. 2023. Rare EIF4A2 variants are associated with a neurodevelopmental disorder characterized by intellectual disability, hypotonia, and epilepsy. *Am J Hum Genet* **110**:120–145.

Rajan A, Housden BE, Wirtz-Peitz F, Holderbaum L, Perrimon N. 2017. A Mechanism Coupling Systemic Energy Sensing to Adipokine Secretion. *Dev Cell* **43**:83-98 e6.

Rajan A, Perrimon N. 2012. Drosophila cytokine unpaired 2 regulates physiological homeostasis by remotely controlling insulin secretion. *Cell* **151**:123–137.

Rangel Silvares R, Nunes Goulart da Silva Pereira E, Eduardo Ilaquita Flores E, Lino Rodrigues K, Ribeiro Silva A, Gonçalves-de-Albuquerque CF, Daliry A. 2019. High-fat diet-induced kidney alterations in rats with metabolic syndrome: endothelial dysfunction and decreased antioxidant defense. *Diabetes Metab Syndr Obes* **12**:1773–1781.

Recasens-Alvarez C, Ferreira A, Milán M. 2017. JAK/STAT controls organ size and fate specification by regulating morphogen production and signalling. *Nat Commun* **8**:13815.

Ruggiero C, Ehrenshaft M, Cleland E, Stadler K. 2011. High-fat diet induces an initial adaptation of mitochondrial bioenergetics in the kidney despite evident oxidative stress and mitochondrial ROS production. *American Journal of Physiology-Endocrinology and Metabolism* **300**:E1047–E1058.

Sánchez-Navarro A, Martínez-Rojas MÁ, Caldiño-Bohn RI, Pérez-Villalva R, Zambrano E, Castro-Rodríguez DC, Bobadilla NA. 2021. Early triggers of moderately high-fat diet-induced kidney damage. *Physiol Rep* **9**:e14937.

Schneider CA, Rasband WS, Eliceiri KW. 2012. NIH Image to ImageJ: 25 years of image analysis. *Nat Methods* **9**:671–675.

Serrano E, Shenoy P, Martinez Cantarin MP. 2023. Adipose tissue metabolic changes in chronic kidney disease. *Immunometabolism (Cobham)* **5**:e00023.

Sisler JD, Morgan M, Raje V, Grande RC, Derecka M, Meier J, Cantwell M, Szczepanek K, Korzun WJ, Lesnefsky EJ, Harris TE, Croniger CM, Larner AC. 2015. The signal transducer and activator of transcription 1 (STAT1) inhibits mitochondrial biogenesis in liver and fatty acid oxidation in adipocytes. *PLoS One* **10**:e0144444.

Struhl G, Basler K. 1993. Organizing activity of wingless protein in Drosophila. *Cell* **72**:527–540.

Sun Y, Ge X, Li Xue, He J, Wei X, Du J, Sun J, Li Xin, Xun Z, Liu W, Zhang H, Wang Z-Y, Li YC. 2020. High-fat diet promotes renal injury by inducing oxidative stress and mitochondrial dysfunction. *Cell Death Dis* **11**:1–14.

Szeto HH, Liu S, Soong Y, Alam N, Prusky GT, Seshan SV. 2016. Protection of mitochondria prevents high-fat diet-induced glomerulopathy and proximal tubular injury. *Kidney Int* **90**:997–1011.

Thomas S, Fisher KH, Snowden JA, Danson SJ, Brown S, Zeidler MP. 2015. Methotrexate Is a JAK/STAT Pathway Inhibitor. *PLoS One* **10**:e0130078.

Tsuboi N, Koike K, Hirano K, Utsunomiya Y, Kawamura T, Hosoya T. 2013. Clinical features and long-term renal outcomes of Japanese patients with obesity-related glomerulopathy. *Clin Exp Nephrol* **17**:379–385.

Tuttle KR, Brosius FC 3rd, Adler SG, Kretzler M, Mehta RL, Tumlin JA, Tanaka Y, Haneda M, Liu J, Silk ME, Cardillo TE, Duffin KL, Haas JV, Macias WL, Nunes FP, Janes JM. 2018. JAK1/JAK2 inhibition by baricitinib in diabetic kidney disease: results from a Phase 2 randomized controlled clinical trial. *Nephrol Dial Transplant* **33**:1950–1959.

US Department of Health and Human Services, Centers for Disease Control and Prevention (Atlanta, GA). 2023. Chronic Kidney Disease in the United States, 2023. *Centers for Disease Control and Prevention*. https://www.cdc.gov/kidneydisease/publications-resources/ckd-national-facts.html

van de Leemput J, Wen P, Han Z. 2022. Using Drosophila Nephrocytes to Understand the Formation and Maintenance of the Podocyte Slit Diaphragm. *Front Cell Dev Biol* **10**:837828.

van der Heijden RA, Bijzet J, Meijers WC, Yakala GK, Kleemann R, Nguyen TQ, de Boer RA, Schalkwijk CG, Hazenberg BPC, Tietge UJF, Heeringa P. 2015. Obesity-induced chronic inflammation in high fat diet challenged C57BL/6J mice is associated with acceleration of age-dependent renal amyloidosis. *Sci Rep* **5**:1–15.

Wang L, Wen P, van de Leemput J, Zhao Z, Han Z. 2021. Slit diaphragm maintenance requires dynamic clathrin-mediated endocytosis facilitated by AP-2, Lap, Aux and Hsc70-4 in nephrocytes. *Cell Biosci* **11**:83.

Weavers H, Prieto-Sánchez S, Grawe F, Garcia-López A, Artero R, Wilsch-Bräuninger M, Ruiz-Gómez M, Skaer H, Denholm B. 2009. The insect nephrocyte is a podocyte-like cell with a filtration slit diaphragm. *Nature* **457**:322–326.

Wen P, Zhang F, Fu Y, Zhu J-Y, Han Z. 2020. Exocyst Genes Are Essential for Recycling Membrane Proteins and Maintaining Slit Diaphragm in Drosophila Nephrocytes. *J Am Soc Nephrol* **31**:1024–1034.

Woodcock KJ, Kierdorf K, Pouchelon CA, Vivancos V, Dionne MS, Geissmann F. 2015. Macrophage-derived upd3 cytokine causes impaired glucose homeostasis and reduced lifespan in Drosophila fed a lipid-rich diet. *Immunity* **42**:133–144.

Yamout H, Lazich I, Bakris GL. 2014. Blood pressure, hypertension, RAAS blockade, and drug therapy in diabetic kidney disease. *Adv Chronic Kidney Dis* **21**:281–286.

Zhang F, Zhao Y, Chao Y, Muir K, Han Z. 2013a. Cubilin and amnionless mediate protein reabsorption in Drosophila nephrocytes. *J Am Soc Nephrol* **24**:209–216.

Zhang F, Zhao Y, Han Z. 2013b. An in vivo functional analysis system for renal gene discovery in Drosophila pericardial nephrocytes. *J Am Soc Nephrol* **24**:191–197.

Zhang H, Nair V, Saha J, Atkins KB, Hodgin JB, Saunders TL, Myers MG Jr, Werner T, Kretzler M, Brosius FC. 2017. Podocyte-specific JAK2 overexpression worsens diabetic kidney disease in mice. *Kidney Int* **92**:909–921.

Zhao F, Zhu J-Y, Richman A, Fu Y, Huang W, Chen N, Pan X, Yi C, Ding X, Wang S, Wang P, Nie X, Huang J, Yang Y, Yu Z, Han Z. 2019. Mutations in NUP160 Are Implicated in Steroid-Resistant Nephrotic Syndrome. *J Am Soc Nephrol* **30**:840–853.

Zhao Y, Cocco C, Domenichini S, Samson ML, Rabinow L. 2015. The IMD innate immunity pathway of Drosophila influences somatic sex determination via regulation of the Doa locus. *Dev Biol* **407**:224–231.

Zhao Y, Duan J, Han ID, van de Leemput J, Ray PE, Han Z. 2024. Piezo, nephrocyte function, and slit diaphragm maintenance in Drosophila. *J Am Soc Nephrol*. doi:10.1681/ASN.0000000529

Zhao Y, Duan J, van de Leemput J, Han Z. 2023a. Cardiac neurons expressing a glucagon-like receptor mediate cardiac arrhythmia induced by high-fat diet in Drosophila. *bioRxiv*. doi:10.1101/2023.12.13.571403

Zhao Y, Johansson E, Duan J, Han Z, Alenius M. 2023b. Fat- and sugar-induced signals regulate sweet and fat taste perception in Drosophila. *Cell Rep* **42**:113387.

Zhao Y, Khallaf MA, Johansson E, Dzaki N, Bhat S, Alfredsson J, Duan J, Hansson BS, Knaden M, Alenius M. 2022. Hedgehog-mediated gut-taste neuron axis controls sweet perception in Drosophila. *Nat Commun* **13**:7810.

Zhu J-Y, Fu Y, Richman A, Zhao Z, Ray PE, Han Z. 2017. A Personalized Model of COQ2 Nephropathy Rescued by the Wild-Type COQ2 Allele or Dietary Coenzyme Q10 Supplementation. *J Am Soc Nephrol* **28**:2607–2617.

Zhuang S, Shao H, Guo F, Trimble R, Pearce E, Abmayr SM. 2009. Sns and Kirre, the Drosophila orthologs of Nephrin and Neph1, direct adhesion, fusion and formation of a slit diaphragm-like structure in insect nephrocytes. *Development* **136**:2335–2344.

FIGURE LEGENDS

Figure 1. High-fat diet compromises nephrocyte function

Nephrocytes from control *Drosophila* (w^{1118}, females) fed a regular diet (normal fat diet, NFD) or high-fat diet (NFD supplemented with 14% coconut oil, HFD) for 7 days from eclosion. **(A)** Representative confocal images of nephrocytes show green fluorescence indicative of FITC-albumin uptake. Scale bar: 50 µm. **(B)** Box plot shows the quantitation of the relative fluorescence intensity of FITC-albumin shown in (A); middle line depicts the median and whiskers show minimum to maximum. Statistical analysis was performed with a two-tailed Student's t-test; ****, P<0.0001; n = 6 flies. **(C)** Representative confocal images of *Drosophila* nephrocytes (w^{1118}, 7-day old females) show red fluorescence indicative of 10 kD dextran uptake. Scale bar: 50 µm. **(D)** Box plot shows the quantitation of the relative fluorescence intensity of 10 kD dextran shown in (C); middle line depicts the median and

whiskers show minimum to maximum. Statistical analysis was performed with a two-tailed Student's t-test; **, P<0.01; n = 6 flies.

Figure 2. High-fat diet changes nephrocyte morphology

Nephrocytes from control *Drosophila* (w^{1118}, 7-day-old females) fed a regular diet (normal fat diet, NFD) or high-fat diet (NFD supplemented with 14% coconut oil, HFD). **(A)** Representative confocal images of *Drosophila* nephrocytes immunostained with anti-polychaetoid (Pyd) in green. Upper panels show cortical surface; Scale bar: 5 µm. Lower panels show subcortical regions; Scale bar: 5 µm. **(B)** Quantitation of Pyd protein distribution (cytoplasmic vs membrane); middle line depicts the median and whiskers show minimum to maximum. Statistical analysis was performed with a two-tailed Student's t-test; ***, P<0.001; n = 8 nephrocytes (1 nephrocyte/fly) from 7-day-old female flies. **(C)** Transmission electron microscopy (TEM) images of *Drosophila* nephrocyte (w^{1118}, 7-day-old females) cortical regions. Scale bar: 0.5 µm. **(D)** Quantitation of lacuna channel (LC)-LC distance based on images in (C); middle line depicts the median and whiskers show minimum to maximum. Statistical analysis was performed with a two-tailed Student's t-test; **, P<0.01; n = 60 LC-LC distance measurements obtained in 10 nephrocytes from six 7-day-old female flies for each group. **(E)** TEM images of *Drosophila* nephrocyte (w^{1118}, 7-day-old-females) cytoplasmic regions. Red asterisks indicate large vacuoles. Scale bar: 0.5 µm. **(F)** Quantitation of the vacuoles that contain electron dense structures based on images in (E). The middle line depicts the median and whiskers show minimum to maximum. Statistical analysis was performed with a two-tailed Student's t-test; ****, P<0.0001; n = 12 nephrocytes for NFD and 29 nephrocytes for HFD from six 7-day-old female flies.

Figure 3. High-fat diet activates the JAK-STAT pathway in nephrocytes

(A) Table lists human genes encoding JAK-STAT pathway components, along with their *Drosophila* homologs, the DRSC Integrative Ortholog Prediction Tool (DIOPT) score (maximum score = 15), and their function. **(B)** Graphical representation of the JAK-STAT signaling pathway and interaction between its components. Domeless, Dome; JAK Hopscotch, Hop; Signal-transducer and activator of transcription 92E, Stat92E; Suppressor of cytokine signaling at 36E, Socs36E; Unpaired, Upd. **(C)** Representative confocal images of nephrocytes from control *Drosophila* (*10xStat92E*-GFP, 7-day-old females) fed a regular diet (normal fat diet, NFD) or high-fat diet (HFD, NFD supplemented with 14% coconut oil). *10xStat92E*-GFP is shown in green fluorescence; DAPI (blue) stains DNA to visualize the nucleus. Scale bar: 50 µm. **(D)** Box plot shows the quantitation of the relative fluorescence

intensity of *10xStat92E*-GFP based on images in (C); middle line depicts the median and whiskers show minimum to maximum. Statistical analysis was performed with a two-tailed Student's t-test; ***, P<0.001; n = 6 flies.

Figure 4. JAK-STAT pathway activation compromises nephrocyte function

(A) Schematic illustration of targeted UAS-*hop.Tum* expression in the nephrocytes; *hopscotch.Tumorous-lethal*, dominant gain-of-function, constitutively activates JAK-STAT. Temperature sensitive Gal80ts binds to Gal4 and acts as a negative regulator of the Gal4 transcriptional activator at 18°C. A temperature switch to 29°C releases Gal80ts inhibition as it can no longer bind Gal4, thus allowing UAS-*hop.Tum* expression driven by Gal4 to occure. Timeline for temperature switches of the fly at different stages of development have been indicated. **(B)** Representative confocal images of FITC-albumin fluorescence (green) in nephrocytes from control flies (*Dot*-Gal4/+; *tub*-Gal80ts/+) and those with activated JAK-STAT (*Dot*-Gal4/UAS-*hop.Tum*; *tub*-Gal80ts/+). Scale bar: 50 µm. **(C)** Box plot shows the quantitation of the relative fluorescence intensity of FITC-albumin based on images in (B); middle line depicts the median and whiskers show minimum to maximum. Statistical analysis was performed with a two-tailed Student's t-test; ****, P<0.0001; n = 6 flies (7-day-old females). **(D)** Representative confocal images of 10 kD dextran fluorescence (red) in nephrocytes from control flies (*Dot*-Gal4/+; *tub*-Gal80ts/+) and those with activated JAK-STAT (*Dot*-Gal4/UAS-*hop.Tum*; *tub*-Gal80ts/+); DAPI (blue) stains DNA to visualize the nucleus. Scale bar: 50 µm. **(E)** Box plot shows the quantitation of the relative fluorescence intensity of 10 kD dextran uptake based on images in (D); middle line depicts the median and whiskers show minimum to maximum. Statistical analysis was performed with a two-tailed Student's t-test; **, P<0.01; n = 6 flies (7-day-old females). **(F)** Schematic illustration of the Flp-out clone strategy to induce UAS-*hop.Tum* expression. Heat shock induces the expression of Flp recombinase, which excises a stop cassette to initiate Gal4 expression. Gal4 binding to the upstream activation sequences (UAS) drives the expression of GFP (as a marker for positive Flp-out clones) and UAS-*hop.Tum*. **(G)** Representative confocal images of 10 kD dextran fluorescence (red) in nephrocytes from flies with a GFP labelled Flp-out UAS-*hop.Tum* clone (*hs-Flp*^{122}/+; UAS-*Flp*^{JD1}/UAS-*hop.Tum*; *Act5C>CD2>Gal4*^{S}, UAS-*mCD8GFP*^{LL6}/+). **(H)** Box plot shows the quantitation of the relative fluorescence intensity of 10 kD dextran fluorescence uptake based on images in (G); middle line depicts the median and whiskers show minimum to maximum. Control (neighbor of Flp-out clone; UAS-*hop.Tum* (clone). Statistical analysis was performed with a two-tailed Student's t-test; ****, P<0.0001; n= 5 clones and 5 neighbor cells.

Figure 5. Silencing *Socs36E* in the nephrocytes, or *upd2* overexpression in the fat body, leads to nephrocyte dysfunction

(A) Representative confocal images of FITC-albumin (green) in nephrocytes from control flies (*Dot*-Gal4/+) and flies with nephrocyte-specific silencing of the Socs36E JAK-STAT inhibitor (*Dot*-Gal4>*Socs36E*-IR); DAPI (blue) stains DNA to visualize the nucleus. Scale bar: 50 µm. *Socs36E*, *Suppressor of cytokine signaling at 36E*. **(B)** Box plot shows the quantitation of the relative fluorescence intensity of FITC-albumin uptake based on images in (A); middle line depicts the median and whiskers show minimum to maximum. Statistical analysis was performed with a two-tailed Student's t-test; **, P<0.01; n= 6 flies (7-day-old females). **(C)** Representative confocal images of 10 kD dextran fluorescence (red) in nephrocytes from control flies (*Dot*-Gal4/+) and flies with nephrocyte-specific silencing of the Socs36E JAK-STAT inhibitor (*Dot*-Gal4>*Socs36E*-IR); DAPI (blue) stains DNA to visualize the nucleus. Scale bar: 50 µm. *Socs36E*, *Suppressor of cytokine signaling at 36E*. **(D)** Box plot shows the quantitation of the relative fluorescence intensity of 10 kD dextran uptake based on images in (C); middle line depicts the median and whiskers show minimum to maximum. Statistical analysis was performed with a two-tailed Student's t-test; ***, P<0.001; n= 6 flies (7-day-old females). **(E)** Representative confocal images of 10 kD dextran fluorescence (red) in nephrocytes from control flies (*ppl*-Gal4/+) and flies with fat body-specific overexpression of JAK-STAT ligand Upd2 (*ppl*-Gal4>*upd2-GFP*); DAPI (blue) stains DNA to visualize the nucleus. Scale bar: 50 µm. *ppl*, *pumpless*; *upd2*, *unpaired 2*. **(F)** Box plot shows the quantitation of the relative fluorescence intensity of 10 kD dextran uptake based on images in (E); middle line depicts the median and whiskers show minimum to maximum. Statistical analysis was performed with a two-tailed Student's t-test; ****, P<0.0001; n= 6 flies (7-day-old females). **(G)** Representative confocal images of nephrocytes from control flies (*ppl-Gal4/*+) and flies with fat body-specific overexpression of Upd2 (*ppl-Gal4>upd2-GFP*). Anti-Pyd is shown in red. Scale bar: 4 µm. **(H)** Quantitation of Pyd protein distribution (cytoplasmic vs membrane); middle line depicts the median and whiskers show minimum to maximum. Statistical analysis was performed with a two-tailed Student's t-test; ****, P<0.0001; n = 12 nephrocytes (1 nephrocyte/fly) from 7-day-old female flies.

Figure 6. Silencing *Stat92E* attenuates nephrocyte functional defects caused by a high-fat diet

Nephrocytes from control flies (*Dot*-Gal4/+; *tub*-Gal80ts/+) and those with *Stat92E* silencing as adults (*Dot*-Gal4/UAS-*Stat92E*-IR; *tub*-Gal80ts/+). UAS-*Stat92E*-RNAi expression was induced at the adult stage (see Figure 4A) for seven days before the uptake assay. *Stat92E*, *Singal-transducer and activator of transcription 92E*. **(A)** Representative confocal images of

FITC-albumin fluorescence (green); DAPI (blue) stains DNA to visualize the nucleus. Scale bar: 50 µm. **(B)** Box plot shows the quantitation of the relative fluorescence intensity of FITC-albumin uptake based on images in (A); middle line depicts the median and whiskers show minimum to maximum. Statistical analysis was performed by two-way ANOVA with Sidak correction; **, P<0.01; ****, P<0.0001; ns, not significant; n = 6 flies (7-day-old females). **(C)** Representative confocal images of 10 kD dextran fluorescence (red); DAPI (blue) stains DNA to visualize the nucleus. Scale bar: 50 µm. **(D)** Box plot shows the quantitation of the relative fluorescence intensity of 10 kD dextran uptake based on images in (C); middle line depicts the median and whiskers show minimum to maximum. Statistical analysis was performed by two-way ANOVA with Sidak correction; ***, P<0.001; ****, P<0.0001; ns, not significant; n = 6 flies (7-day-old females).

Figure 7. Methotrexate treatment can restore nephrocyte function following a high-fat diet

Nephrocytes from control *Drosophila* (w^{1118}; 7-day-old females) fed a regular diet (normal fat diet, NFD) or high-fat diet (NFD supplemented with 14% coconut oil, HFD), with or without methotrexate (10 µM; ex vivo 60 min) treatment. **(A)** Representative confocal images of FITC-albumin fluorescence (green). Scale bar: 50 µm. **(B)** Box plot shows the quantitation of the relative fluorescence intensity of FITC-albumin uptake based on images in (A); middle line depicts the median and whiskers show minimum to maximum. Statistical analysis was performed by two-way ANOVA with Sidak correction; ***, P<0.001, ****, P<0.0001; ns, not significant; n = 6 flies (7-day-old females). **(C)** Representative confocal images of 10 kD dextran fluorescence (red). Scale bar: 50 µm. **(D)** Box plot shows the quantitation of the relative fluorescence intensity of 10 kD dextran uptake based on images in (C); middle line depicts the median and whiskers show minimum to maximum. Statistical analysis was performed by two-way ANOVA with Sidak correction; ****, P<0.0001; ns, not significant; n = 6 flies (7-day-old females). **(E)** Graphic of proposed model for high-fat diet-induced nephrocyte defects via an adipose-nephrocyte axis. A high-fat diet upregulates the expression and secretion of the adipokine Unpaired 2 (Upd2), leptin-like hormone, from the fat body. Upd2 is a JAK-STAT ligand, and it activates JAK-STAT signaling at the nephrocytes (Signal-transducer and activator of transcription 92E, Stat92E; Suppressor of cytokine signaling at 36E, Socs36E; JAK Hopscotch, Hop; Domeless, Dome). The overactive JAK-STAT pathway disrupts the integrity of the slit diaphragm (SD) filtration structure and thereby leads to nephrocyte dysfunction.

Figure 1

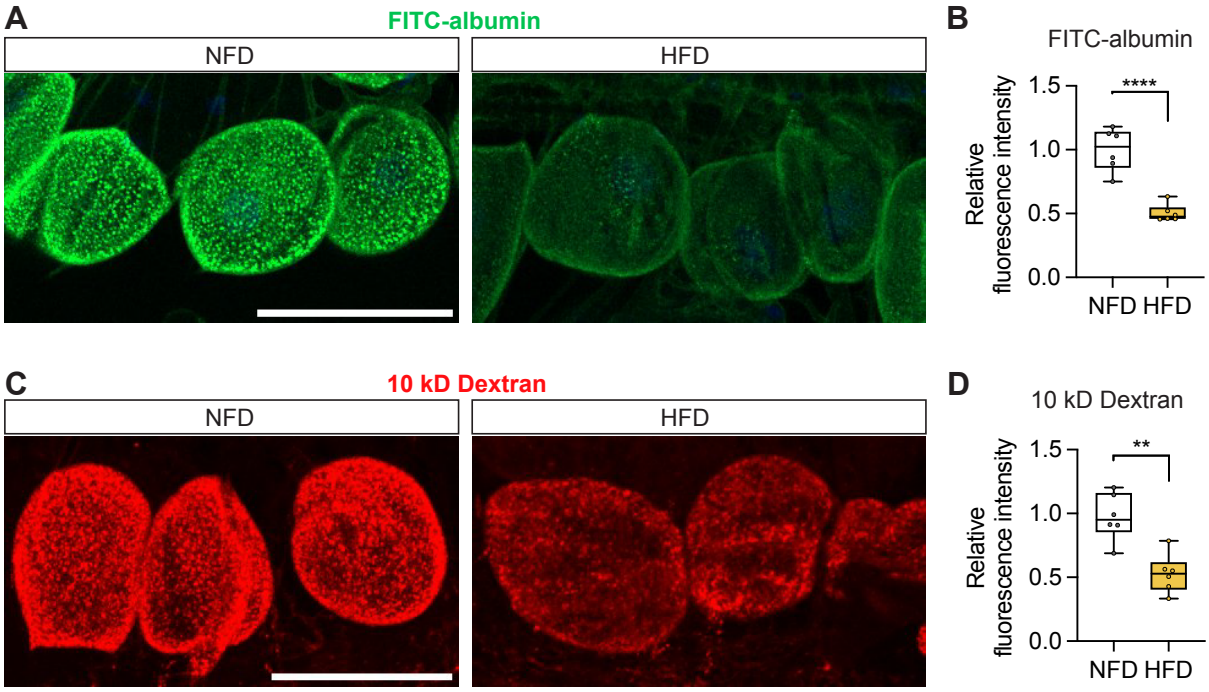
A
FITC-albumin
NFD
HFD
B
FITC-albumin
Relative fluorescence intensity
1.5
1.0
0.5
0.0
****
NFD HFD
C
10 kD Dextran
NFD
HFD
D
10 kD Dextran
Relative fluorescence intensity
1.5
1.0
0.5
0.0
**
NFD HFD

Figure 2

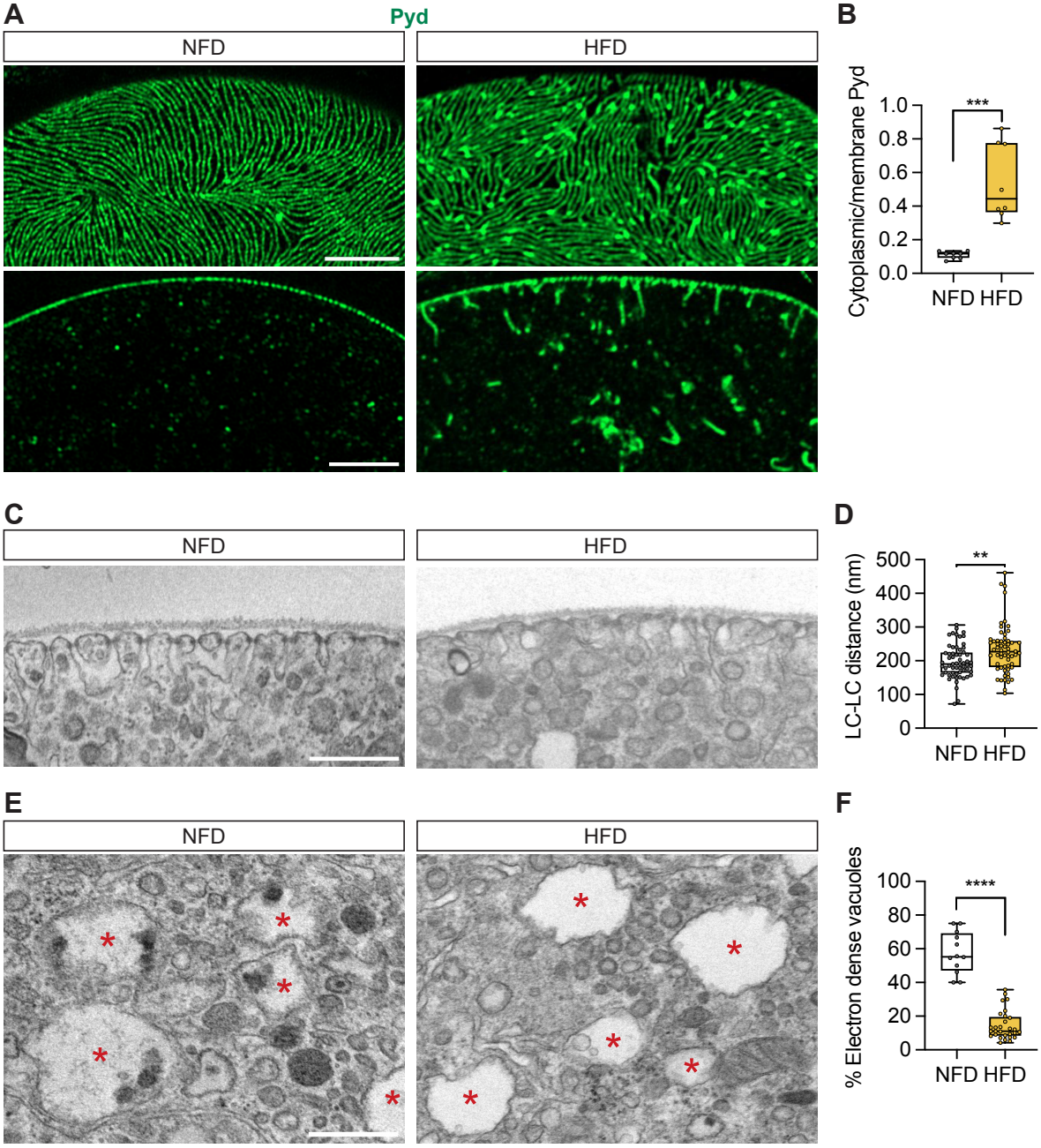
A
Pyd
NFD
HFD
B
Cytoplasmic/membrane Pyd
1.0
0.8
0.6
0.4
0.2
0.0
***
NFD HFD
C
NFD
HFD
D
LC-LC distance (nm)
500
400
300
200
100
0
**
NFD HFD
E
NFD
HFD
F
% Electron dense vacuoles
100
80
60
40
20
0
****
NFD HFD

Figure 3

A

Human Gene	*Drosophila* Homolog	DIOPT Score	Function
STAT5B	*Stat92E*	13	transcription factor
PTPRQ	*dome*	2	transmembrane receptor
JAK1/JAK2	*hop*	11	non-receptor tyrosine kinase
SOCS4/SOCS5	*Socs36E*	7	negative regulator of JAK-STAT

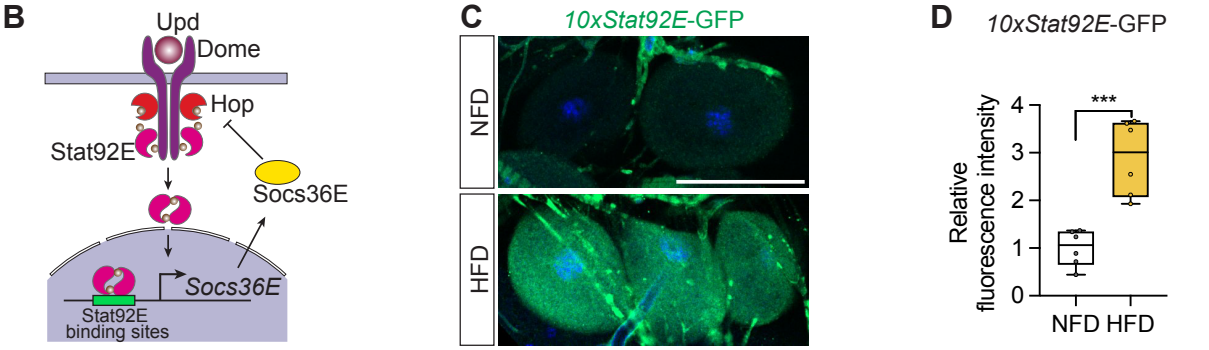

Figure 4

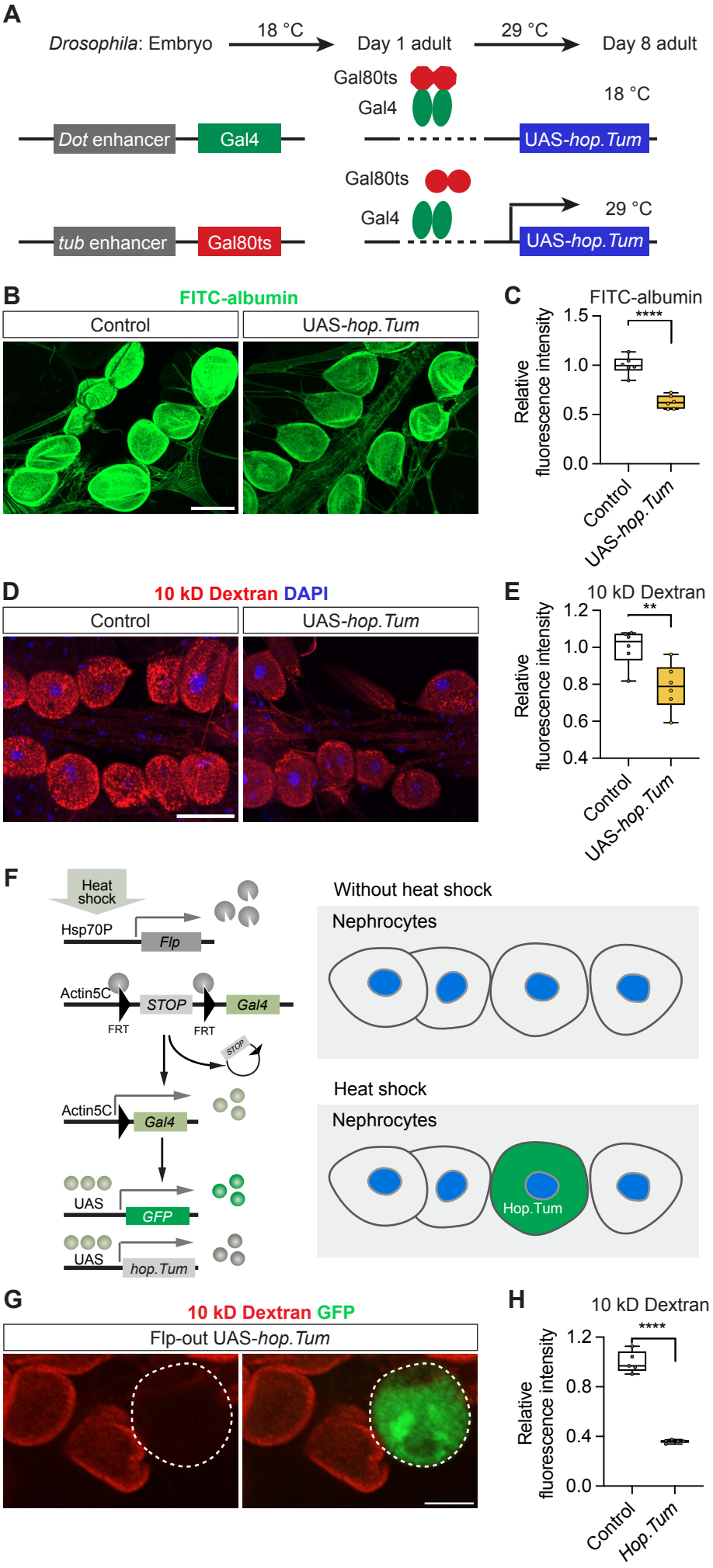
A
Drosophila: Embryo
18 °C
Day 1 adult
29 °C
Day 8 adult
Gal80ts
Gal4
18 °C
Dot enhancer
Gal4
UAS-hop.Tum
Gal80ts
Gal4
29 °C
tub enhancer
Gal80ts
UAS-hop.Tum
B
FITC-albumin
Control
UAS-hop.Tum
C
FITC-albumin
Relative fluorescence intensity
1.5
1.0
0.5
0.0
****
Control
UAS-hop.Tum
D
10 kD Dextran DAPI
Control
UAS-hop.Tum
E
10 kD Dextran
Relative fluorescence intensity
1.2
1.0
0.8
0.6
0.4
**
Control
UAS-hop.Tum
F
Heat shock
Hsp70P
Flp
Actin5C
STOP
Gal4
FRT
FRT
STOP
Actin5C
Gal4
UAS
GFP
UAS
hop.Tum
Without heat shock
Nephrocytes
Heat shock
Nephrocytes
Hop.Tum
G
10 kD Dextran GFP
Flp-out UAS-hop.Tum
H
10 kD Dextran
Relative fluorescence intensity
1.2
0.8
0.4
0.0
****
Control
Hop.Tum

Figure 5

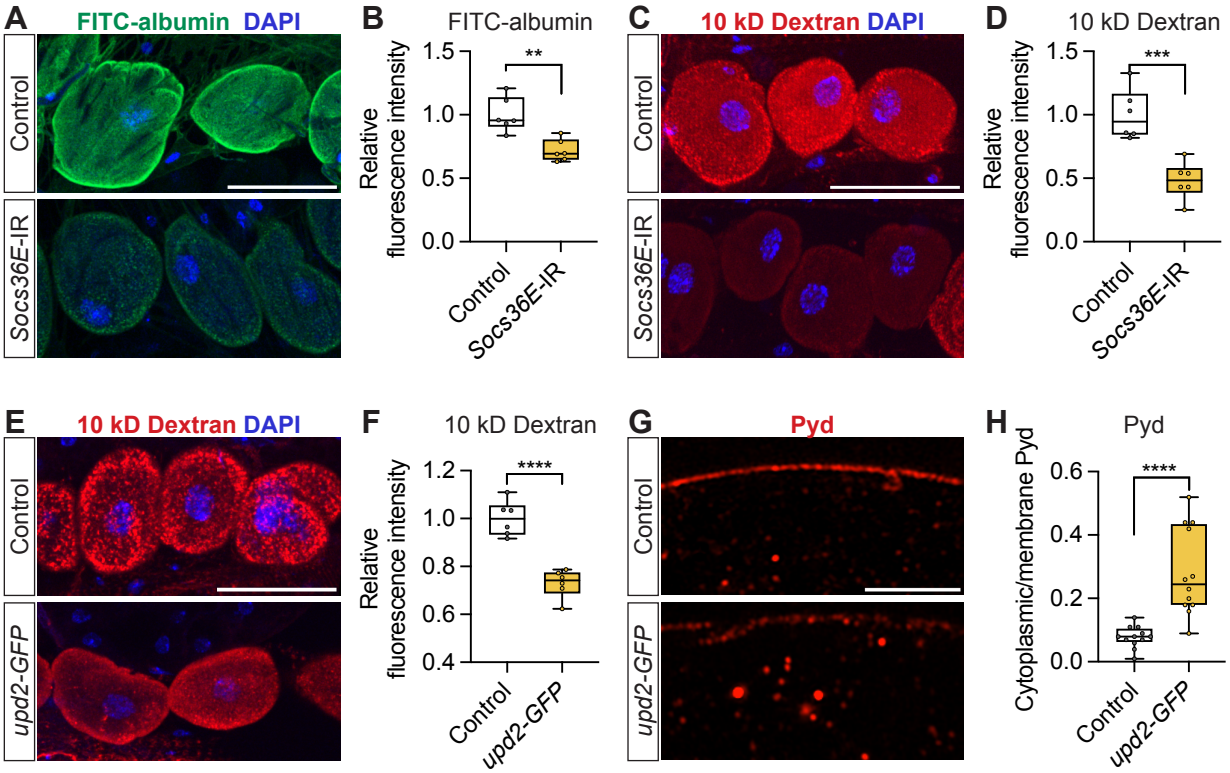
A
FITC-albumin DAPI
Control
Socs36E-IR
B
FITC-albumin
Relative fluorescence intensity
1.5
1.0
0.5
0.0
**
Control
Socs36E-IR
C
10 kD Dextran DAPI
Control
Socs36E-IR
D
10 kD Dextran
Relative fluorescence intensity
1.5
1.0
0.5
0.0
***
Control
Socs36E-IR
E
10 kD Dextran DAPI
Control
upd2-GFP
F
10 kD Dextran
Relative fluorescence intensity
1.2
1.0
0.8
0.6
0.4
****
Control
upd2-GFP
G
Pyd
Control
upd2-GFP
H
Pyd
Cytoplasmic/membrane Pyd
0.6
0.4
0.2
0.0
****
Control
upd2-GFP

Figure 6

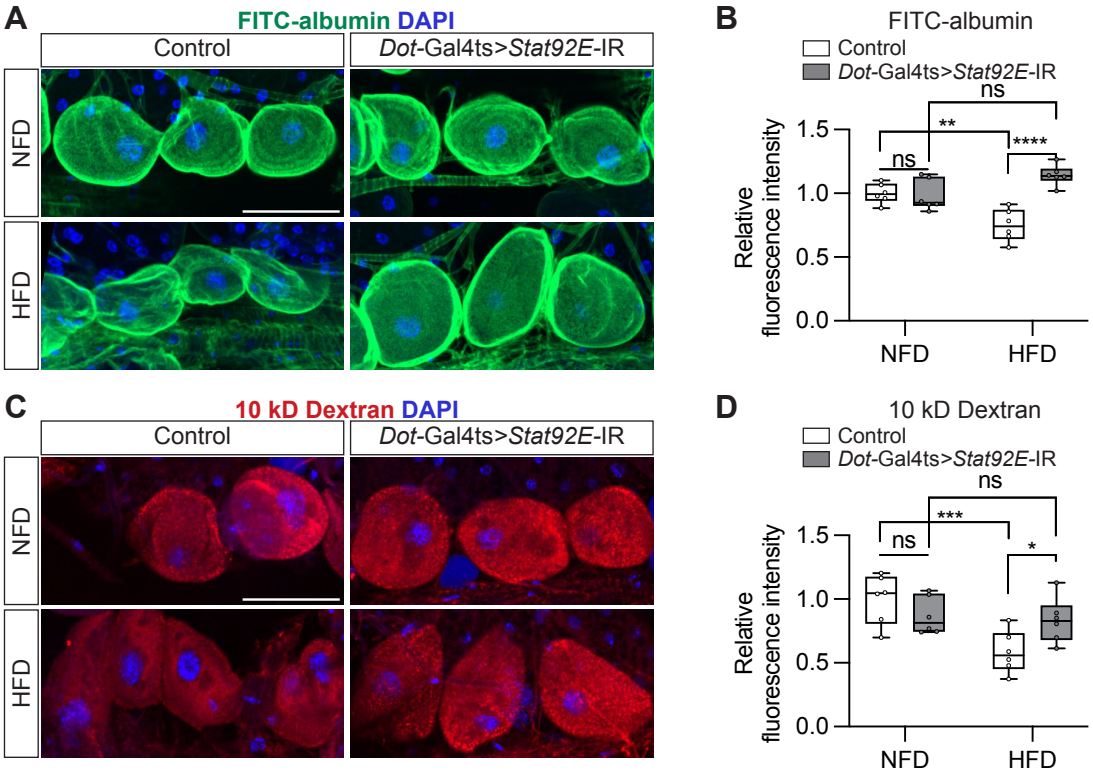
A
FITC-albumin DAPI
Control
Dot-Gal4ts>Stat92E-IR
NFD
HFD
B
FITC-albumin
Control
Dot-Gal4ts>Stat92E-IR
Relative fluorescence intensity
1.5
1.0
0.5
0.0
ns
**
ns
****
NFD
HFD
C
10 kD Dextran DAPI
Control
Dot-Gal4ts>Stat92E-IR
NFD
HFD
D
10 kD Dextran
Control
Dot-Gal4ts>Stat92E-IR
Relative fluorescence intensity
1.5
1.0
0.5
0.0
ns
***
ns
*
NFD
HFD

Figure 7

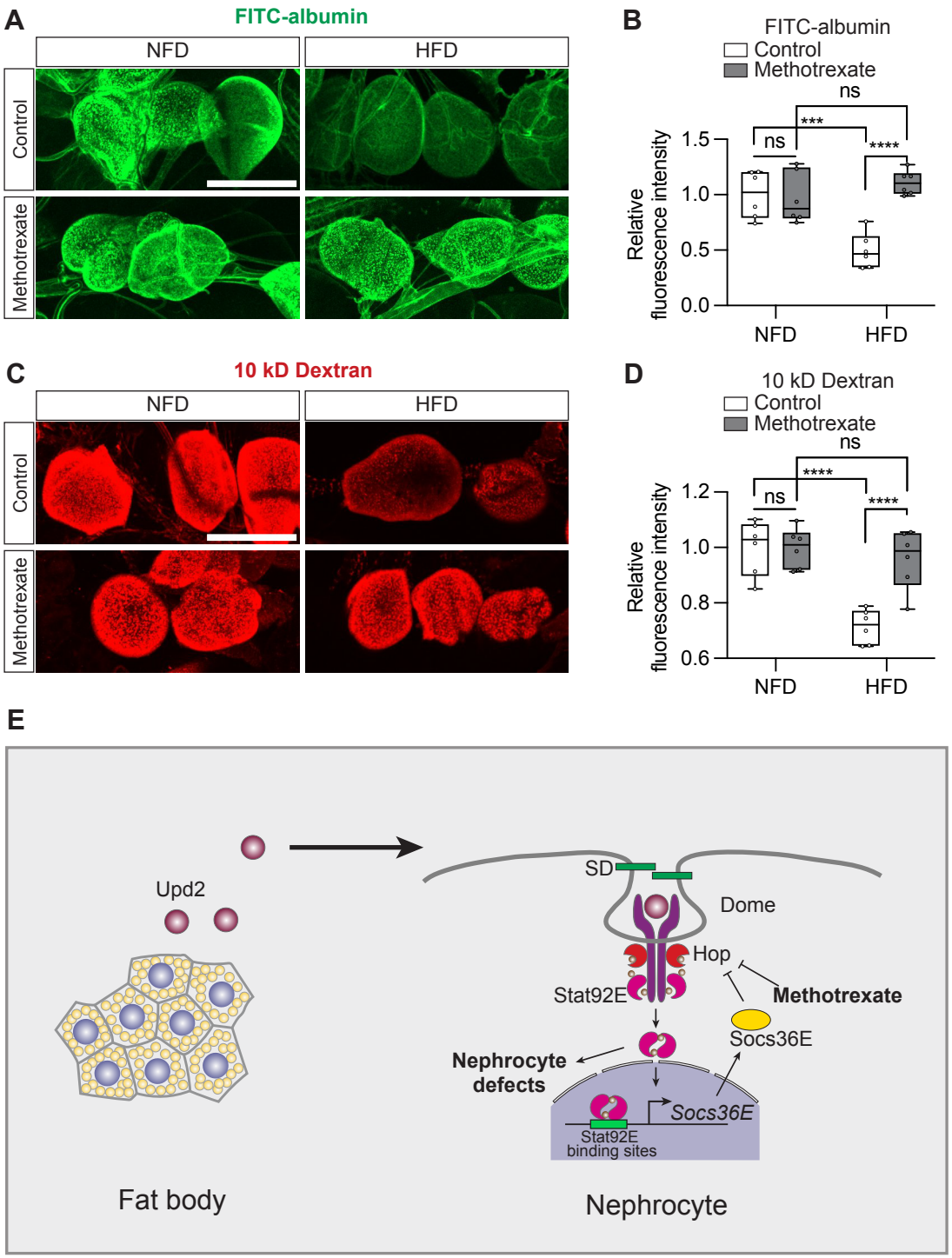
A
FITC-albumin
NFD
HFD
Control
Methotrexate
B
FITC-albumin
Control
Methotrexate
ns
***
ns
****
Relative fluorescence intensity
1.5
1.0
0.5
0.0
NFD
HFD
C
10 kD Dextran
NFD
HFD
Control
Methotrexate
D
10 kD Dextran
Control
Methotrexate
ns
****
ns
****
Relative fluorescence intensity
1.2
1.0
0.8
0.6
NFD
HFD
E
Upd2
SD
Dome
Hop
Stat92E
Methotrexate
Socs36E
Nephrocyte defects
Socs36E
Stat92E binding sites
Fat body
Nephrocyte